

## Working hardening behaviors of severely cold deformed and fine-grained AZ31 Mg alloys at room temperature

CHAO Hong-ying, SUN Hong-fei, WANG Er-de

School of Materials Science and Engineering, Harbin Institute of Technology, Harbin 150001, China

Received 10 May 2011; accepted 25 July 2011

**Abstract:** AZ31 Mg alloy extrusion wires were drawn to a maximum cumulative area reduction of 61% at room temperature, and the 61%-drawn sample was subjected to various annealing treatments for grain refinement. Tensile tests were performed on all the as-drawn and as-annealed samples at a constant strain rate at room temperature. The entire stress–strain curves of each investigated sample were analyzed for the dependence on drawn area reduction and mean grain size. The results show that the cold drawn samples exhibit a constant elastic modulus; however, the stresses are significantly dependent on the deformation level. The corresponding  $\theta$ – $\sigma$  curves (where  $\theta$  is the strain hardening rate,  $d\sigma/d\varepsilon$ ) show extended stage II and suppressed stage IV of strain hardening. The recrystallized samples exhibit enhanced yield stress with the grain size refinement and typical hardening stages of polycrystalline metals: II, III, IV and V. Additionally, decreasing in stage IV with refining grain size is observed probably due to the contribution of grain boundaries slipping. The different hardening behaviors demonstrate the various hardening mechanisms between the cold drawn and recrystallized materials.

**Key words:** AZ31 magnesium alloys; work hardening; cold drawing; grain size; cold deformation

### 1 Introduction

Magnesium alloys have attracted significant interest due to their excellent specific properties and low density, which make these materials potentially suitable for applications in some automobile and electronics parts [1–3]. However, the poor formability of Mg and Mg alloys restricts their severe plastic deformation at room temperature due to their hexagonal close-packed (HCP) structure. Researches on the room deformation behaviors of Mg alloys can be hardly seen [4]. Considerable attention has been focused on the room deformation behaviors of Mg alloys by tension or compression tests, where the true strain, less than 0.3, was obtained in the fine-grained materials [5–9]. The limited deformations supported by tension and compression tests are not enough for the study of severe plasticity deformation in Mg alloys. Recently, LIANG et al [10–11] reported that cold extrusion at room temperature was successfully processed on AZ31 Mg alloy sheets and rods. The microstructures were refined to 1.6  $\mu\text{m}$  and 1.9  $\mu\text{m}$  for the sheets and rods, respectively. This conventional manufacturing method offers possibility of study on the

room deformation behaviors of Mg alloys in a relatively broad plasticity range more than 0.3.

Work hardening behavior is one of the important characteristics in the cold plastic deformation process of materials at room temperature [12]. Up to now, many researches have dedicated to the effects of temperature, strain rate and texture on work hardening of Mg alloys [2, 7, 9, 13–15], but it seems that there is no detailed study about effects of large strain more than 0.5 and grain size on work hardening at room temperature. In the present study, refined AZ31 Mg alloy wires obtained by extrusion were subjected to cold drawing at room temperature. Various drawn area reductions were obtained with a maximum value of 61% which was equivalent to true strain of 0.94. Then the drawn deformation effect on work hardening was investigated by means of tension test at room temperature. To accurately understand the fine grain size dependence on work hardening, the 61% drawn materials were annealed at various heat treatments for further grain size refinement, and then the hardening behaviors of the as-annealed and as-received (or commonly called as-recrystallized) AZ31 Mg alloys were analyzed as well.

The materials used in the present study were a hot extrusion fabricated AZ31 Mg alloy wire with a diameter of 2 mm. Figure. 1 shows the microstructure of the as-received material consisted of equiaxed grains with a mean linear intercept grain size of  $(9.5\pm 0.5)\ \mu\text{m}$ . Then it was followed by cold drawing processing with each passed area reduction of 8%–12% ( $\varphi = [1 - (d_{n+1}/d_n)^2] \times 100\%$ , where  $n$  is the number of processing passes,  $d$  is the diameter of wire and  $\varphi$  is the area reduction of each pass). Cold drawing was performed on an AZ31 wire until it began to fracture in order to achieve the maximum drawn area reduction. According to the relationship of  $\varepsilon = \ln(d_n/d_0)^2$  (where  $d_n$  is the wire diameter via  $n$  processing passes and  $d_0$  is the starting diameter), drawn deformation of 61% was corresponded to true strain value of 0.94. The 61%-drawn sample was then annealed at 250 °C for 60 min and at 300 °C for 10 min to achieve equiaxed and recrystallized microstructures with various refined grain sizes.

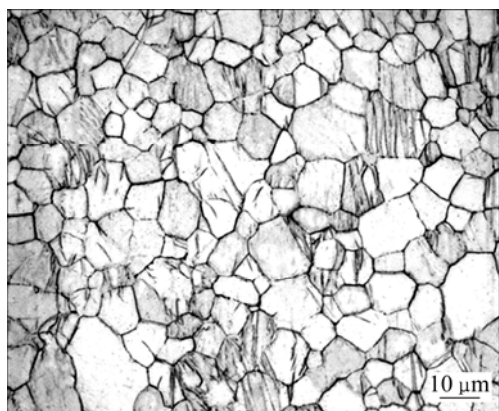


**Fig. 1** Microstructure of as-received AZ31 Mg alloy

The microstructures of all the drawn and recrystallized samples were measured using an Olympus PMG3 optical microscope. The mean grain size was calculated using a linear intercept method, and thousands of grains were taken into account for the evaluation. To investigate the effects of grain size and drawn deformation on work hardening, uniaxial tensile tests were carried out at room temperature with a constant initial strain rate of  $1.67 \times 10^{-3}\ \text{s}^{-1}$ . The valid gauge diameters of all the specimens were the same as their own diameters and the gauge length was 10 mm. The tensile direction was parallel to the extrusion and drawing direction.

## 2 Results

### 2.1 Microstructural characterization

Figure 2 shows the microstructure evolution of AZ31 Mg alloy during cold drawing process. Profuse

twinning activity occurred at 10%-drawn sample. This is in accordance with the observation of VALLE et al [2] who reported increasing twinning activity occurred after larger strains of 5% and 15%. However, they did not give microstructure evolution at larger strains more than 15%. Figure. 2(a) shows nearly 90% grains contained deformation twinning at a drawn reduction of 23.4%. As deformation proceeded, more grains are elongated to form a fiber structure (Fig. 2(b)), which is the characteristic of cold drawn materials and indicated abundantly stored dislocations. According to the phenomenological Kocks model [16–18], the dislocation activities, including the accumulation of forest dislocation and the annihilation of dislocation, were the cause of strain hardening for FCC metals. For HCP metals, however, grain size and twinning may also play an important role in strain hardening except for dislocations since the compact relationship of hardening behavior and microstructures [17]. The volume fraction, shape, orientation and arrangement of defects and grain boundaries can be identified as microstructural features.

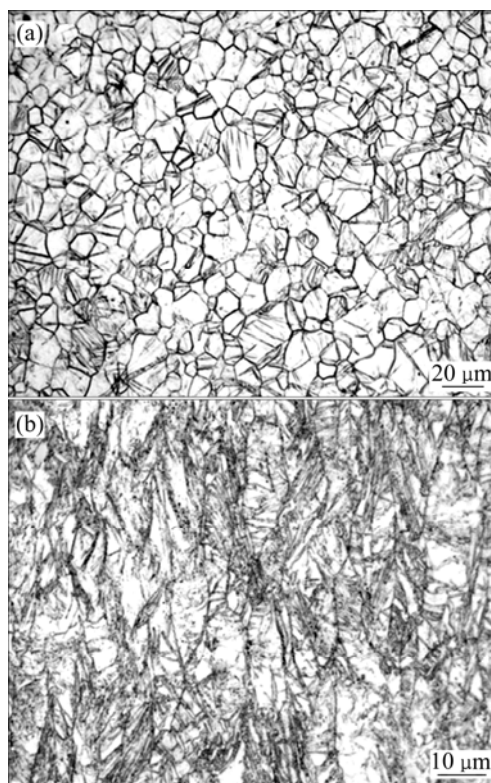


**Fig. 2** Microstructure evolution in drawing process at room temperature at various drawn area reductions: (a)  $\varphi = 23.4\%$ ; (b)  $\varphi = 61.0\%$

Upon annealing, the deformed microstructures of the 61%-drawn samples were replaced by equiaxed and small recrystallized grains with the average grain sizes of 3.8  $\mu\text{m}$  and 4.5  $\mu\text{m}$  at 250 °C for 60 min and 300 °C for 10 min, respectively, as shown in Figs. 3(a) and (b).

Such a group of annealed materials were selected for the aim of eliminating the texture effect on strain hardening, which was based on the fundamental knowledge that slight annealing treatments had little effect on the texture components and intensity. As a result, only the grain size effect was taken into consideration.

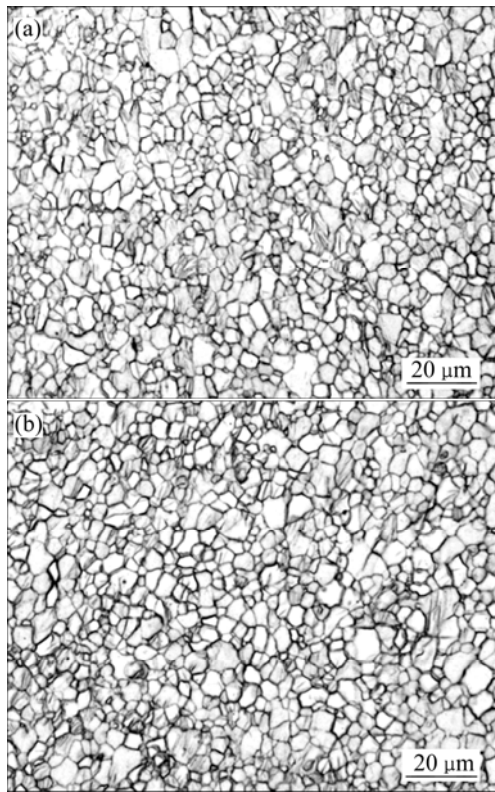


**Fig. 3** Microstructures of 61%-drawn AZ31 upon annealing treatments: (a) 250 °C, 60 min; (b) 300 °C, 10 min

## 2.2 Tensile flow stress—strain curves

The schematic curves of true stress versus true strain for the as-drawn samples and the recrystallized samples are shown in Fig. 4. It can be seen that for the given loading model in Fig. 4(a), a close correlation between microstructures and mechanical properties exists, i.e., yield strengths (YS) and ultimate tensile strengths (UTS) are greatly increased with the drawn deformation while opposite to the ductility. For example, the YS ( $\sigma_{0.2}$ ) and UTS ( $\sigma_b$ ) reach 376 MPa and 477 MPa at 61%, exhibiting a strong enhancement of approximate 100% in YS compared with as-received material. The ductility, however, tends to be very poor with the elongation less than 2% to failure. The state of drawn deformation seems to play a critical role. In addition, in all the investigated cases there is a steep increase in flow stress at the initial tensile deformation below about 1%, followed by a plateau with a maximum stress value. It results in an decreased and high yield-to-tensile strength ratio between 0.72 and 0.8 with drawn deformation, and a high equal elastic module about 40 GPa as well. This

kind of observation has also been seen in steels [17, 19] and aluminum alloys [20], which is similar to the Bauschinger effect.

Grain size dependence of tensile properties for the recrystallized materials is obvious as expected from the Hall-Petch relation. The YS values have a significant increase with the decrease of the grain size, as shown in Fig. 4(b). Refining the grain size from about 10  $\mu\text{m}$  to 3.8  $\mu\text{m}$ , the YS raises by about 35%, whereas the UTS value keeps a constant value of about 330 MPa, which exhibits again a decreased yield-to-tensile strength ratio. The increased yield stress should be ascribed to the grain boundaries strengthening effect at the initial plasticity deformation stage. The influence of deformation twinning on the YS is not as valid as reported in the twinning-induced steels [21] and coarse-grained Mg alloys [22], although profuse twinning is present in the as-received material.

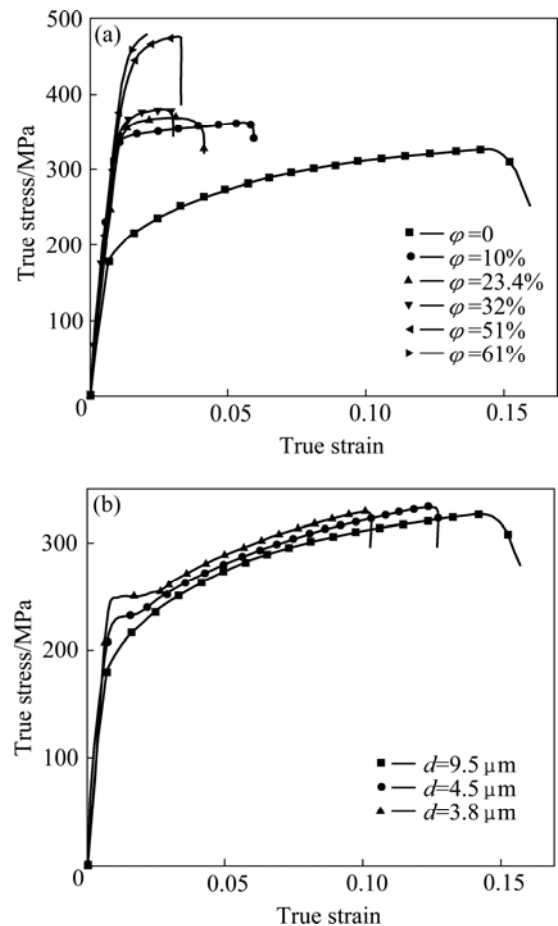


**Fig. 4** True stress—strain curves of as-drawn and as-received (a) and as-annealed AZ31 alloy (b) samples tested at a constant strain rate of  $1.67 \times 10^{-3} \text{ s}^{-1}$  at room temperature

## 3 Discussion

### 3.1 Strain hardening behaviors of as-drawn specimens

In this section, the influence of cold drawn deformation on the strain hardening behaviors of

deformed AZ31, in the area reduction range from 0 to 61%, was investigated based on the model of Kocks-Mecking [16, 18]. The universal expression of this model was given:

$$\tau - \tau_0 = \alpha \mu b \rho^{1/2} \quad (1)$$

where  $\tau_0$  is the critical resolved shear stress;  $\alpha$  is a coefficient, assumed independent of the strain;  $\mu$  is the shear modulus;  $b$  is the Burgers vector of the dislocations;  $\rho$  is the dislocation density. The rate of dislocation accumulation with the shear strain  $\gamma$  can be expressed as:

$$\frac{d\rho}{d\gamma} = \frac{1}{bL} \quad (2)$$

where  $L$  stands for dislocation mean free path, the most important factor of dislocation accumulation. When moving dislocations interact with grain boundaries, twin boundaries and other dislocations, the mean free path becomes:

$$\frac{1}{L} = \frac{1}{D_0} + \frac{1}{D} + \frac{\rho^{1/2}}{\beta} \quad (3)$$

where  $D_0$  is the initial grain size and  $D$  is the mean twinning spacing. In this paper, because of the small grain size ( $d < 10 \mu\text{m}$ ), decrease of the deformation twinning fraction and the absence of twinning in the refined recrystallized materials, the difference between  $D_0$  and  $D$  can be neglected and then Eq. (3) can be recognized as  $(1/L) = (1/D) + (\rho^{1/2}/\beta)$ . For the un-drawn samples with low dislocation density, therefore, the initial grain size determines the yield strength. Setting  $L \propto D_0$ , Eqs. (2) and (3) lead to  $\rho \propto D_0^{-1}$  and then  $\sigma \propto D_0^{-1/2}$ , i.e., grain size dependence of strain hardening. Alternatively, for the severely drawn samples, owing to the densification of the forest of dislocations,  $L$  quickly becomes smaller than  $D_0$  and the overall strain hardening behaviour is grain size-independent. Integration of Eq. (2) leads to  $\rho \propto \varepsilon^2$ , furthermore,  $\sigma \propto \varepsilon$ , i.e., a linear increase of flow stress with strain.

Another form of Kocks hardening model can be comprehensible by  $\tau\theta$  through differentiation of Eq. (1) with respect to the strain yields; when the grain size is small at the submicron level, there is:

$$\tau\theta = (\tau - \tau_0) \frac{d\tau}{d\gamma} = \frac{(\alpha\mu)^2 b}{2} \frac{1}{L} \quad (4)$$

where  $\theta = d\tau/d\gamma$ , indicating the shear hardening due to storage of dislocations.

Combined with Eq. (3), the strain hardening rate becomes:

$$\frac{\theta}{\mu} = \frac{\alpha}{2\beta} + \frac{\alpha}{2D_0\rho^{1/2}} \quad (5)$$

Eq. (6) implies that the strain-hardening rate should

be a defined fraction of the shear modulus and the effect of dislocation hardening can be ignored as a consequence of small dislocation density, just as in the fully recrystallized materials. These analyses will be used in Figs. 5 and 6 to assess the effect of drawing deformation on strain hardening behaviour in the plots of  $\theta$ - $\varepsilon$  and  $\theta$ - $\tau$ .

Figure 5 shows the  $\sigma$ - $\varepsilon$  behaviors of the drawn specimens in the forms of difference values of yield strength,  $\Delta\sigma$  ( $=\sigma_{i+1}-\sigma_i$ ), and yield ratio ( $\sigma_{0.2}/\sigma_b$ ) versus the equivalent true strain. It well describes the strong strain dependence of yield strength especially at the severely drawn deformations. After drawing deformation, all the samples show increased yield up to 0.86 in comparison with 0.56 of the as-received material. Both higher yield strength and yield ratio result in difficulties in further deformation in the following plasticity deformed process, such as acquiring higher drawn area reductions.

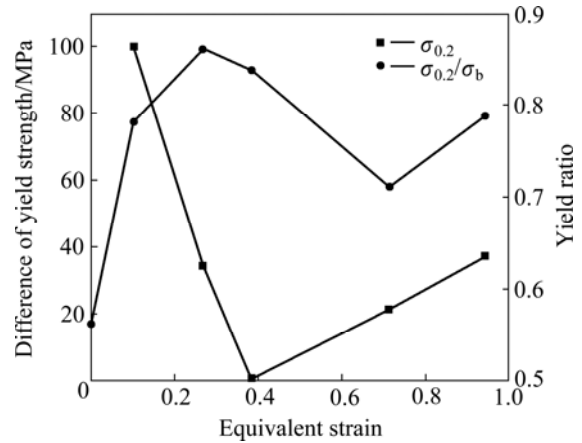


**Fig. 5** Drawing deformation dependence of difference of yield strength  $\Delta\sigma$  ( $\Delta\sigma = \sigma_{i+1} - \sigma_i$ ) and yield ratio ( $\sigma_{0.2}/\sigma_b$ ) for drawn specimens

Figure 6 shows a set of strain hardening rates,  $\theta$ , as a function of tensile strain (Fig. 6(a)) and flow stress (Fig. 6(b)) for the drawn specimens. It is shown that they all start with a similarly steep decrease at small strains and then approach a steady state with a very low hardening rate in the  $\theta$ - $\varepsilon$  curves, which is in accordance with the plateau in the stress-strain curves. The  $\theta$ - $(\sigma - \sigma_{0.2})$  curves of the as-drawn specimens in Fig. 6(b) exhibit the same difference from the undrawn one. The former develops broad stage II of strain hardening but suppressed stage IV, while the latter has typical hardening features composed of stages II-V. This means, with the increase of stress, the hardening rate decreases gradually to zero at an enlarged extent for the drawn materials, while a relatively steady region is presented in a large stress range for the as-received sample followed by  $\theta$ -value decreasing to 0. Assumed the strain hardening rate in the plateaus is defined to be the thermal strain

hardening rate, it exhibits 1.5 GPa for the as-received material in this study but a much less value close to 0 for all the drawn specimens. It is declared that the strain hardening behaviors of deformed materials are completely different from the as-received sample, although it seems that both are induced by dislocation evolution. The stored dislocations in the drawn materials significantly influence the subsequent dislocation activity which determines the hardening behaviors measured by tensile tests. Such influence may turn to pin the movement of dislocations but not to hinder dislocation generation. Consequently, the applied stress for the severely deformed material is higher than the slightly deformed one at the same strain level. However, the hardening rate may be similar to each other, as shown in Figs. 5 and 6. The higher the deformation, the stronger the effect probably.

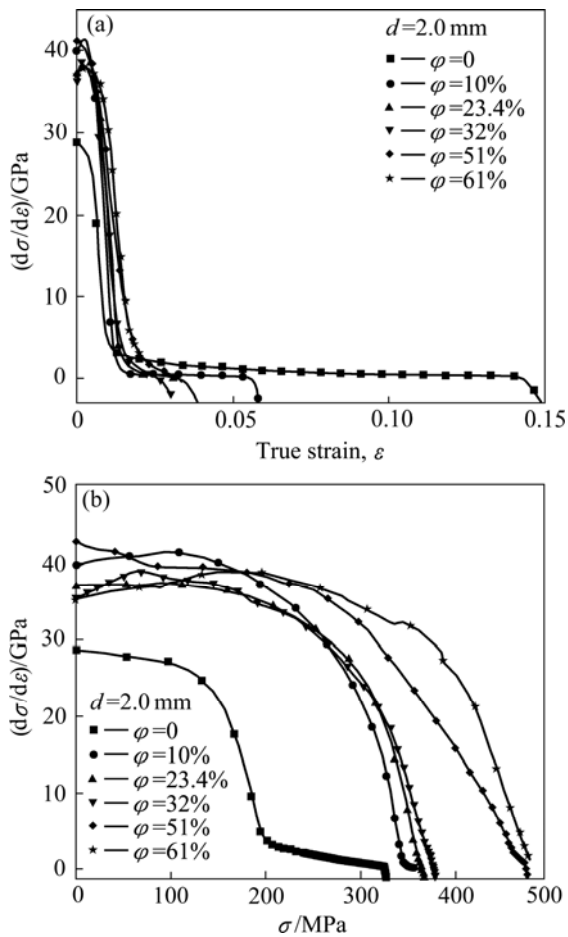


**Fig. 6** Drawn deformation dependence of hardening rate in plots of (a)  $\theta-\varepsilon$ , and (b)  $\theta-\sigma$  for drawn AZ31 Mg alloy materials

**3.2 Strain hardening behaviors of recrystallized specimens**

As described above, the hardening behaviors of both the deformed and the as-received AZ31 alloys were

greatly different. Therefore, the recrystallized materials were re-analyzed using Kocks-Mecking’s hardening model. Here, emphasis was put on the grain size effect since the twinning effect and texture effect can be ignorable through the microstructure observation.

Figure 7 shows the strain hardening behaviors in the forms of  $\theta-(\sigma-\sigma_{0.2})$  for grain sizes ranging from 2.4  $\mu\text{m}$  to 9.5  $\mu\text{m}$ . A clear straight drop at low flow stress is seen for all the samples, as reported in Refs [1, 2, 5, 17], which is recognized as the thermal stage III of strain hardening. At this stage, the decrease of  $\theta$  is produced with the increase of the net flow stress. As stage III appears to approach a saturation level, the new stage IV intervenes when the hardening rate has dropped to a particular value, the average value of which is 1.5 GPa  $\approx \mu/10$  for these studied samples, where  $\mu$  (15.5 GPa) is the average shear module. In addition, smaller grain size shows a lower stress at the inflexion point linked stage III than stage IV, i.e., the refinement of the grain size leads to a decrease in hardening rate in stage IV. It is also reported that the ECAE-ed AZ31 exhibits an increasing  $\theta_{IV}$  with the decrease of the grain size due to twinning effect [23]. VALLE et al [2] reported the same interesting observation in AZ31 Mg alloy, whereas the opposite that increasing hardening rate with grain size refinement was also seen in the same stage IV in AZ61, which was described as  $\theta_0^{III}$  to be a hardening limit extrapolated to  $\sigma=0$ . In B.C.C steel, it was demonstrated the higher  $\theta_{IV}$  resulted from both the finer grain size and smaller precipitates [17]. The contradiction among these reports is mainly due to their respective characteristic of the microstructures such as the second phase, the chemical contents and the defects. In the present study, the AZ31 Mg alloys are single-phase solid solution without considering the solid strengthening effect, additionally, twins are only visible in the as-received material. Low twinning formation is observed in the refined annealed samples. As a result, the decrease in

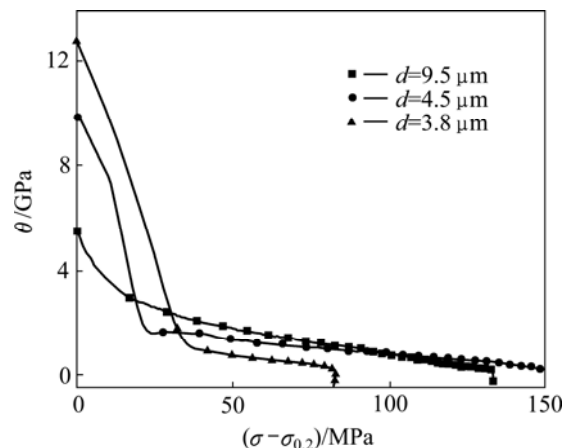


**Fig. 7**  $\theta$  vs  $(\sigma-\sigma_{0.2})$  for as-received and as-annealed AZ31 Mg alloy samples

strain hardening rate especially in the stage IV with the refinement in grain size cannot be ascribed to a decrease in twinning activity, but probably caused by constraints of neighboring grains [2] rather than by an increase in dynamic recovery at room temperature. Such an explanation has been demonstrated by VALLE [2] and KOIKE et al [24] who reported the occurrence of grain boundaries in  $d=8\ \mu\text{m}$  AZ31 alloy deformed at room temperature. When  $\theta$  reaches 0 at a higher stress, a separate stage V appears with a steady state situation at  $\theta=0$ . ZEHETBAUER et al [25–26] attributed such a stage to point defect generation and absorption. The observation of tensile samples in this text indicates damage accumulation at this stage with continuous deformation rather decreasing stress, as the stress—strain curves shown in Fig. 4(b). It is generally accepted that stage V is strongly dependent on deformation temperature and strain rate. In conclusion, the hardening behaviors of fine-grained AZ31 still obey the common Kocks model but with some variability in stage III where fine grain size seems invalid on the hardening rate. The case is probably due to the grain boundaries slipping in fine microstructures, while the increase in yield stress with decreasing grain size is due to the storage of dislocation at grain boundaries. The decrease in hardening rate limits high deformation in the subsequent plasticity forming processing.

## 4 Conclusions

1) Large strain deformation is developed in AZ31 magnesium alloy in traditional drawing processing at room temperature. Strengths increase significantly with the drawn deformation, showing great influence on the strain hardening behaviors. All the drawn samples show an extended hardening stage II from the beginning of tensile deformation as well as a suppressed stage IV according to Kocks-Mecking model.

2) The grain size refinement in annealed AZ31 results in an increase in yield strength due to the storage of dislocation at grain boundaries, and leads to a decreasing hardening rate in stage IV ascribed to the contribution of grain boundaries slipping induced by the refined grain size, rather than the contribution of twinning effect or texture effect.

## References

- [1] MÁTHIS K, TROJANOVÁ Z, LUKÁČ P. Hardening and softening in deformed magnesium alloys [J]. *Mater Sci Eng A*, 2002, 324: 141–144.
- [2] VALLE J A, del CARREÑO F, RUANO O A. Influence of texture and grain size on work hardening and ductility in magnesium-based alloys processed by ECAP and rolling [J]. *Acta Mater*, 2006, 54: 4247–4259.
- [3] PANICKER R, CHOKSHI A H, MISHRA R K, VERMA R, KRAJEWSKI P E. Microstructural evolution and grain boundary sliding in a superplastic magnesium AZ31 alloy [J]. *Acta Mater*, 2009, 57: 3683–3693.
- [4] STYCZYNSKI A, HARTIG Ch, BOHLEN J, LETZIG D. Cold rolling textures in AZ31 wrought magnesium alloy [J]. *Scripta Mater*, 2004, 50: 943–947.
- [5] WU Hong-yu, LIN Feng-zheng. Mechanical properties and strain-hardening behavior of Mg alloy AZ31B-H24 thin sheet[J]. *Mater Sci Eng A*, 2010, 527: 1194–1199.
- [6] TROJANOVÁ Z, DROZD Z, LUKÁČ P, CHMELÍK F. Deformation behaviour of Mg-Li alloys at elevated temperatures[J]. *Mater Sci Eng A*, 2005, 410–411: 148–151.
- [7] AL-SAMMAN T, GOTTSTEIN G. Room temperature formability of a magnesium AZ31 alloy: Examining the role of texture on the deformation mechanisms [J]. *Mater Sci Eng A*, 2008, 488: 406–414.
- [8] YASUMASA C, HAJIME I, MAMORU M. Stretch formability of AZ31 Mg alloy sheets at different testing temperatures [J]. *Mater Sci Eng A*, 2007, 466: 90–95.
- [9] CÁCERES C H, BLAKE A H. On the strain hardening behaviour of magnesium at room temperature [J]. *Mater Sci Eng A*, 2007, 462: 193–196.
- [10] LIANG S J, LIU Z Y, WANG E D. Microstructure and mechanical properties of Mg-Al-Zn alloy deformed by cold extrusion[J]. *Mater Lett*, 2008, 62: 3051–3054.
- [11] LIANG S J, LIU Z Y, WANG E D. Microstructure and mechanical properties of Mg-Al-Zn alloy sheet fabricated by cold extrusion [J]. *Mater Lett*, 2008, 62: 4009–4011.
- [12] CHEN X H, LU L. Work hardening of ultrafine-grained copper with nanoscale twins [J]. *Scripta Mater*, 2007, 67: 133–136.
- [13] LUKÁČ P, TROJANOVÁ Z. Hardening and softening in selected magnesium alloys [J]. *Mater Sci Eng A*, 2007, 462: 23–28.
- [14] MÁTHIS K, TROJANOVÁ Z, LUKÁČ P, CÁCERES C H, LENDVAI J. Modeling of hardening and softening processes in Mg alloys [J]. *J Alloys Compds*, 2004, 378: 176–179.
- [15] LI M, LOU X Y, KIM J H, WAGONER R H. An efficient constitutive model for room-temperature, low-rate plasticity of annealed Mg AZ31B sheet [J]. *Int J Plasticity*, 2010, 26: 820–858.
- [16] KOCKS U F. Laws for work-hardening and low-temperature creep [J]. *J Eng Mater Technol Trans ASME*, 1976, 98: 76–85.
- [17] FANG X F, DAHL W. Strain hardening of steels at large strain deformation. Part I: Relationship between strain hardening and microstructures of b.c.c. steels [J]. *Mater Sci Eng A*, 1995, 203: 14–25.
- [18] KOCKS U F, MECKING H. Physics and phenomenology of strain hardening: The FCC case [J]. *Prog Mater Sci*, 2003, 48: 171–173.
- [19] YOSHIDA F, UEMORI T. A model of large-strain cyclic plasticity describing the Bauschinger effect and workhardening stagnation [J]. *Int J Plasticity*, 2002, 18: 661–686.
- [20] MOAN G D, EMBURY J D. A study of the bauschinger effect in Al-Cu alloys [J]. *Acta Metall*, 1979, 27: 100–107.
- [21] BOUAZIZ O, ALLAIN S, ESTRIN Y. Effect of pre-strain at elevated temperature on strain hardening of twinning-induced plasticity steels [J]. *Scripta Mater*, 2010, 62: 713–715.
- [22] JIANG L, JONAS J J, LUO A A, SACHDEV A K, GODET S. Influence of {10-12} extension twinning on the flow behavior of AZ31 Mg alloy [J]. *Mater Sci Eng A*, 2007, 445–446: 302–309.
- [23] BARNETT M R, KESHAVARZ Z, BEER A G, ATWELL D. Influence of grain size on the compressive deformation of wrought Mg-3Al-1Zn [J]. *Acta Mater*, 2004, 52: 5093–5103.
- [24] KOIKE J, KOBAYASHI T, MUKAI T, WATANABE H, SUZUKI M, MARUYAMA K, HIGASHI K. The activity of non-basal slip systems and dynamic recovery at room temperature in fine-grained AZ31B magnesium alloys [J]. *Acta Mater*, 2003, 51: 2055–2065.

- [25] ZEHETBAUER M, SEUMER V. Cold work hardening in stages IV and V of FCC metals—I: Experiments and interpretation [J]. Acta Metall Mater, 1993, 41: 577–588.
- [26] ZEHETBAUER M. Cold work hardening in stages IV and V of FCC metals—II: Model fits and physical results [J]. Acta Metall Mater, 1993, 41: 589–599.

## 室温剧烈冷变形和细化 AZ31 镁合金的加工硬化行为

晁红颖, 孙宏飞, 王尔德

哈尔滨工业大学 材料科学与工程学院, 哈尔滨 150001

**摘 要:** 在室温下, 挤压态镁合金丝材最大累计面积减少 61%, 并对所得材料进行退火处理以细化晶粒。在室温下以恒定的应变速率对拉拔态和退火态试样进行拉伸试验, 分析每个试样的拉拔面积减少量和平均晶粒尺寸与整个应力—应变曲线的关系。结果表明: 冷变形试样具有恒定的弹性模量, 但应力明显依赖变形程度。相应的  $\theta$ — $\sigma$  曲线( $\theta$  代表加工硬化速率,  $d\sigma/d\epsilon$ )表现为加工硬化扩展阶段 II 和抑制阶段 IV。再结晶试样随着晶粒的细化屈服应力增高且表现出典型的多晶材料加工硬化阶段: II, III, IV 和 V。此外, 随着晶粒的细化, 由于晶界滑移的作用, 第 IV 阶段出现下降。在冷拉和再结晶材料中, 不同的硬化行为显示出不同的硬化机理。

**关键词:** AZ31 镁合金; 加工硬化; 冷拉拔; 晶粒粒度; 冷变形

(Edited by CHEN Can-hua)